Journal of Palaeogeography, 2026, 15(4): 100368

Available online at www.sciencedirect.com

ScienceDirect

journal homepage: http://www.journals.elsevier.com/journal-of-palaeogeography/

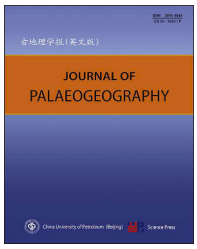

Research article

Sedimentary architecture characteristics and evolutionary patterns of braided-meandering transitional delta

Ming-Qiang Li [a,b], *Da-Li Yue* [a,b,*], *Qin-Xi Tang* [c], *Wu-Rong Wang* [a,b,*], *Qi Wang* [c], *Jia-Rui Zhang* [a,b], *Wei Li* [a,b], *Zi-Mo Xu* [a,b], *Ying-Bo Yuan* [a,b]

[a] *College of Geosciences, China University of Petroleum (Beijing), Beijing, 102249, China*
[b] *State Key Laboratory of Petroleum Resources and Engineering, China University of Petroleum (Beijing), Beijing, 102249, China*
[c] *Great Wall Drilling Company, Sulige Gas Field Branch, China National Petroleum Corporation (CNPC), Ordos, Inner Mongolia, 017300, China*

Abstract Deltaic systems represent one of the major hydrocarbon reservoir types worldwide. However, limited studies of braided-meandering transitional deltas hinder accurate characterization of deltaic sedimentary systems and the efficient development of associated tight-gas reservoirs. Furthermore, this will influence tight-gas recovery during the late development stage of the gas field. To address this issue, this study focuses on the H8 Member of the Guadalupian Shihezi Formation in the Su X Block of the Sulige Gas Field, Ordos Basin, China. An integrated approach combining core observations, well-logging interpretation, seismic inversion, and dynamic data validation is employed to investigate the sedimentary evolution pattern of the braided-meandering transitional delta system. The main findings are as follows: 1) The delta plain is dominated by braided and meandering distributary channels, which are classified into braided channels (sinuosity index <1.3) and meandering channels (sinuosity index >1.3) according to channel sinuosity index. 2) As the base level rises, the braided distributary channels on the delta plain gradually transition to meandering distributary channels. 3) The sand bodies of braided distributary channels are characterized by a cut-and-fill pattern, containing gas-rich reservoirs with higher productivity than those in meandering channels. This study proposes a pattern in which the distributary channels on the delta plain undergo an overall transition from braided to meandering patterns with the local coexistence of both channels. The findings provide a robust theoretical basis for characterizing analogous river-dominated deltaic sedimentary systems and offer meaningful geological guidance for enhancing tight-gas recovery efficiency and optimizing reservoir development strategies in similar petroliferous basins worldwide.

Keywords Delta, Sedimentary architecture, Evolution pattern, Braided-meandering transition, Ordos Basin

* Corresponding authors.
E-mail addresses: yuedali@cup.edu.cn (D.-L. Yue), wwr@cup.edu.cn (W.-R. Wang).
Peer review under responsibility of China University of Petroleum (Beijing)
https://doi.org/10.1016/j.jop.2026.100368

Received 10 October 2025; revised 27 March 2026; accepted 31 March 2026; available online 24 April 2026

1. Introduction

Deltaic reservoirs have long been recognized as key targets in global oil and gas exploration and development, occurring widely in numerous basins such as the Nile Delta Basin (Shehata *et al.*, 2023), the Niger Delta Basin (Ignatius *et al.*, 2025), the Tarim Basin (Zhu *et al.*, 2016), and the Ordos Basin in China (Chu *et al.*, 2023; Pang *et al.*, 2024). The delta plain subfacies, characterized mainly by distributary channels and interchannel, is dominated by sandstone—mudstone interbedding and peat swamp deposits (Syvitski *et al.*, 2005). In river-dominated deltas, frequent channel migration and avulsion, together with localized fine-grained deposition in interchannel or abandoned channel, lead to significant vertical and lateral heterogeneity in reservoir properties (Leila and Moscariello, 2018; Fawad *et al.*, 2023). This heterogeneity not only controls hydrocarbon accumulation and distribution, but also affects fluid flow during production, complicating the spatial pattern of remaining hydrocarbons (Wang *et al.*, 2022; Yang *et al.*, 2023). Therefore, accurately characterizing distributary channels and their internal architectures within delta plains is essential for reducing exploration risk and enhancing the efficiency of reservoir development (García-García *et al.*, 2011; Xu *et al.*, 2025).

Extensive research has been carried out on the sedimentary processes and architectural distribution characteristics of typical braided-river and meandering-river deltas, and relatively systematic sedimentary architecture models have been established (Coleman and Wright, 1975; Galloway, 1975; McPherson *et al.*, 1987; Postma, 1990; Moyano Paz *et al.*, 2020; Celis *et al.*, 2021; Chapkanski *et al.*, 2025). However, numerous distributary channels on river-dominated delta plains are not typical braided or meandering types, but rather transitional forms between meandering and braided channels, namely braided-meandering transitional deltas (García-García *et al.*, 2011; He *et al.*, 2014). At present, researchers have employed satellite imagery, outcrop investigations, and other approaches to examine the planform morphology and sedimentary sequences of braided-meandering transitional deltas (Jorgensen *et al.*, 1990; Bridge, 2003; Li *et al.*, 2022). Nevertheless, the evolutionary pattern of the sedimentary architecture in braided-meandering transitional deltas has yet to be established.

Integration of well-log and seismic data can significantly improve the accuracy of sedimentary architecture characterization (Cao *et al.*, 2025; Ehsan *et al.*, 2025). In this study, considering Block SU X of the Sulige Gas Field in the northern Ordos Basin, China as an example, multi-scale architectural characterization of braided-meandering transitional delta is accomplished by integrating core, logging, seismic, and production data. The current study aims to (1) characterize the distribution of sedimentary architecture of distributary channels in the delta plain; (2) investigate the effects of base-level variations on the evolution of braided-meandering transitional deltas and establish an evolutionary pattern; (3) evaluate the implications of this pattern for hydrocarbon exploration and development. This study integrates well, seismic, and dynamic data to characterize the architectural distribution and establishes the evolutionary patterns of braided-meandering transitional deltas. The insights gained from this study provide valuable guidance for predicting analogous sedimentary systems and for enhancing hydrocarbon recovery in oil and gas fields with comparable sedimentary settings.

2. Geological setting

The Ordos Basin, located in central China, covers an area of approximately 370,000 km^2 (Liu *et al.*, 2022; Jia *et al.*, 2024). From a structural perspective, it is located in the western part of the North China Craton and constitutes a large, superimposed basin with multiple depositional cycles, overlying a crystalline basement of Archean to Paleoproterozoic age. From north to south, the basin is subdivided into six major tectonic units: the Yimeng Uplift, the Western Thrust Belt, the Tianhuan Depression, the Yishan Slope, the Jinxi Flexural Fold Belt, and the Weibei Uplift (Liu *et al.*, 2022; Jia *et al.*, 2024) (Fig. 1A). By the depositional stage of the Lopingian Shiqianfeng Formation, the Paleo-Asian Ocean along the northern margin had closed, initiating continental collision, while tectonic subsidence within the basin

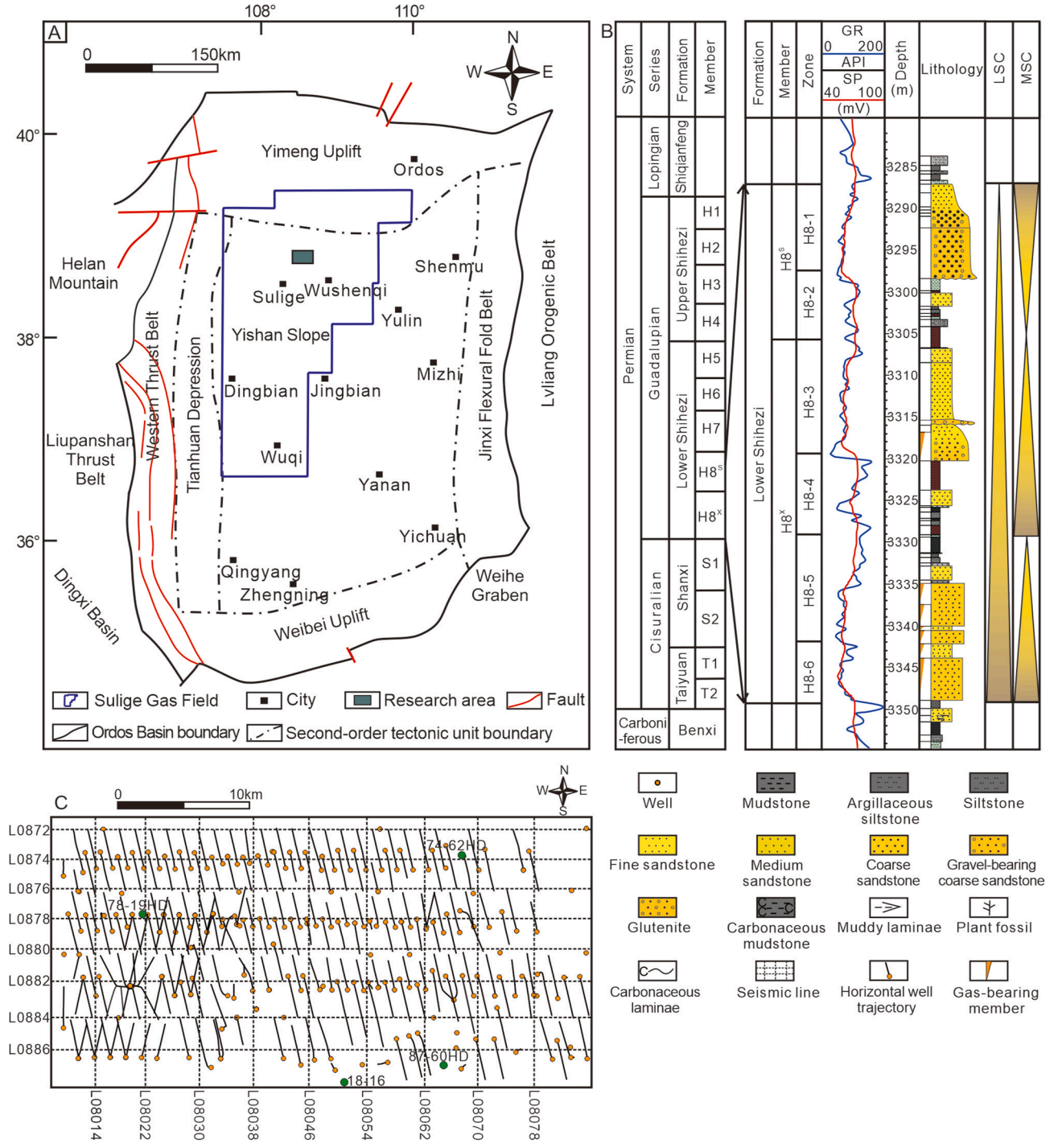

Fig. 1 A) Location and simplified geological map of the Ordos Basin showing major basin features, modified from Yang *et al.* (2008). The blue box highlights the location of the Sulige Gas Field and the green box highlights the location of the research area; B) Comprehensive stratigraphic column of the H8 Member, showing the lithological section, log facies of GR and SP and depositional cycle division, modified from Yang *et al.* (2008); C) Well distribution in the study area. The black line represents the planar projection of the horizontal well trajectory. LSC: Long-term sedimentary cycle. MSC: Mid-term sedimentary cycle.

had significantly slowed. The Guadalupian depositional pattern largely inherited the paleogeographic framework established during the deposition of the Shanxi Formation, characterized by higher topography to the north and south and a relatively depressed central basin. The peripheral uplift belts rose rapidly and expanded in extent, providing abundant sediment supply to the basin (Liu *et al.*, 2020; Chen *et al.*, 2025). During this period, the basin hosted a variety of depositional systems, including alluvial fans, alluvial plains, deltas, and shallow lacustrine facies (Guo *et al.*, 2025; Tao *et al.*, 2025). Toward the end of the Permian, the base level stabilized, lacustrine environments expanded—predominantly in the southern part of the basin—while tidal flat–lagoon systems retreated further south (Guo *et al.*, 2025; Tao *et al.*, 2025).

The study area is situated in the northern part of the Sulige Gas Field, where the primary gas-bearing intervals are Carboniferous and Permian (Fu *et al.*, 2018; Wu *et al.*, 2022). From base to top, the Permian strata in this area comprises the Taiyuan Formation, Shanxi Formation, Shihezi Formation, and Shiqianfeng Formation (Fu *et al.*, 2018; Wu *et al.*, 2022). The Shihezi Formation is divided into the lower and upper formations and further subdivided into eight members (H1–H8) respectively, whereas the Shanxi Formation consists of two members (S1–S2) (Fig. 1B). The present study targets the H8 Member, which has a thickness of approximately 60–85 m and occurs at depths of 3245–3390 m. Structural noses are locally developed, whereas faults are rare (Yin *et al.*, 2018). The regional structural gradient dips from northeast to southwest with ~0.03 rad (Yang *et al.*, 2008). Core and wireline logging data indicate that the H8 Member is a rising long–term cycle, comprising one complete and one rising medium–term cycle (Zhu *et al.*, 2023).

3. Dataset and methodology

3.1. Dataset

By June 2024, a total of 293 wells had been drilled in the study area, including 33 vertical wells, 21 pilot wells, and 228 horizontal wells, of which 11 are sidetracked horizontal wells (Fig. 1C). The Su X Block of the Sulige Gas Field has been developed using a regular horizontal well pattern with a spacing of 600 m × 1200 m.

Seismic coverage in the study area comprises 17 2-D survey lines totaling 253 km, corresponding to a regular acquisition grid spacing of ~1.2 km × 2.4 km (Fig. 1C). The post-stack 2-D seismic data are characterized by a dominant frequency of 19.5 Hz and a bandwidth of 8–29 Hz. The distribution of 2-D seismic lines is shown in Fig. S1, the processed seismic profiles are shown in Fig. S2, and the complete gamma-ray (GR) dataset is shown in Fig. S3 of the Supplementary Material.

In addition, a substantial suite of production performance datasets is available, including bottom-hole pressure measurements, daily individual-well gas-production records, and quantum dot tracer (QDT) test results. This integrated dataset provides a robust multi-disciplinary foundation for sedimentary architecture analysis.

3.2. Seismic data processing and inversion

For clarity, the workflow is subdivided into three components (Fig. 2A, B and C). Seismic responses in the target zone are significantly affected by the responses of the neighboring zones (Li *et al.*, 2023). Multi-wavelet decomposition and reconstruction technology (Ricker, 1953; She *et al.*, 2013) were employed to suppress the strong reflections from the thick coal seams beneath the target interval, thereby improving the quality of seismic data (Fig. 2A). This analysis was implemented using GeoScope 3.7.3 software. The original seismic volume was decomposed into 400 atoms. After removing the first two atoms, the remaining atoms were reconstructed to generate a new seismic volume.

Artificial neural networks (ANNs) have been widely and successfully applied in the field of seismic inversion, improving the interpretation accuracy of research targets (Côrte *et al.*, 2020; Mousavi *et al.*, 2024; Yue *et al.*, 2025a). Specifically, the seismic inversion adopted in this study was realized using the back-propagation neural network (BPNN) (Fig. 2A). The BPNN model for seismic inversion in this study adopted a three-layer structure (input-hidden-output), which included one hidden layer with 13 neurons—this configuration was determined as the optimal solution by comparing different numbers of hidden layers and neurons. The hyperparameters included sigmoid (hidden layer) and linear (output layer) activation functions, the BP algorithm, and training stopping criteria (max 1000 epochs, target MSE 1×10^{-4}, early stop if MSE unchanged for 50 consecutive epochs). Model validation was conducted via 5-fold cross-validation, where quantitative metrics showed good performance with R^2= 0.92 and RMSE = 8 API between predicted and actual GR logs. The BPNN exhibits superior inversion performance with a coefficient of determination (R^2) of 0.92 and a root mean

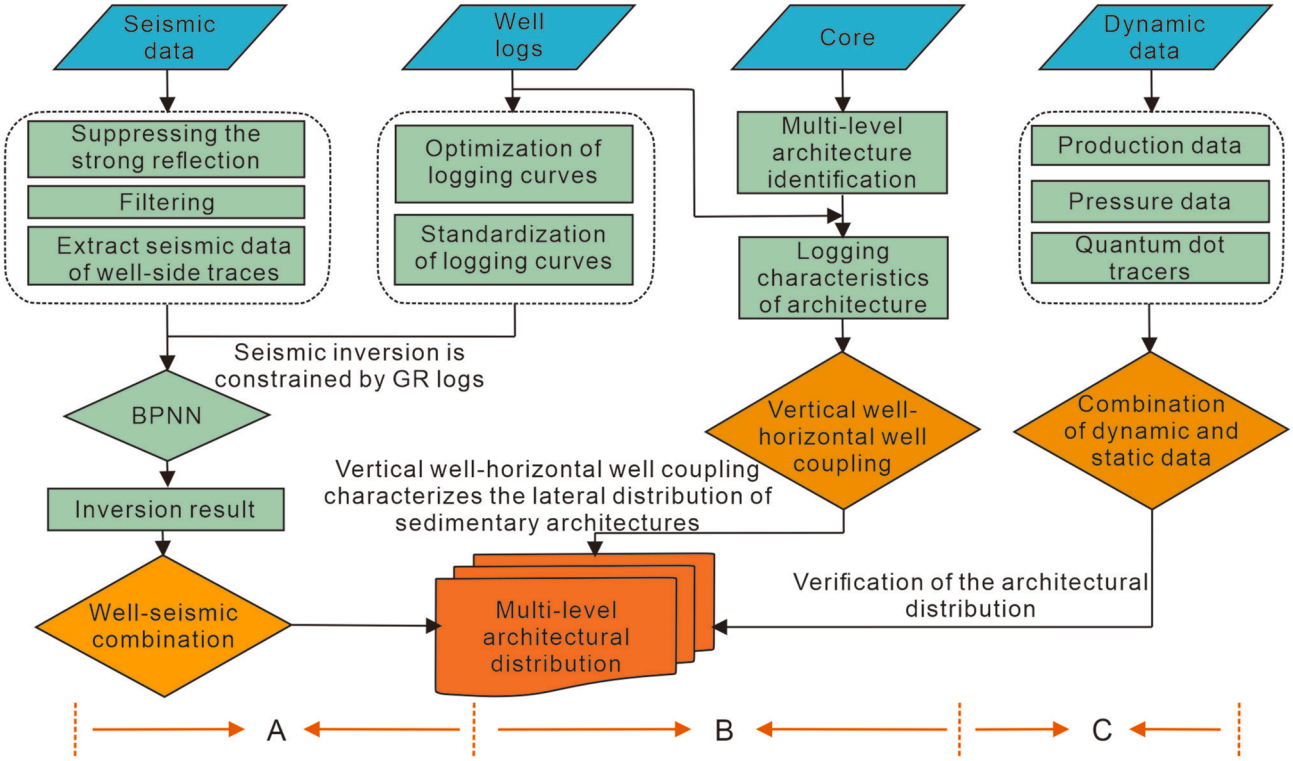

Fig. 2 Workflow diagram outlining the methodology for multi-level architecture characterization of delta plain. It consists of three main methods: seismic data processing and inversion (workflow element A), architectural characterization from well data (workflow element B), and dynamic data validation (workflow element C).

square error (RMSE) of 8 API, significantly outperforming the support vector machine (SVM, R^2= 0.89, RMSE = 9.4 API) and the enhanced artificial neural network (EANN, R^2= 0.84, RMSE = 10.1 API).

The seismic inversion profile constrained by GR logging curves was employed to characterize the lateral distribution of architectural elements in the H8 Member. Specifically, the red (Fig. 3A), green (Fig. 3B), and blue (Fig. 3C) inversion responses correspond to distributary channels, overbanks, and interchannels, respectively.

3.3. Architectural characterization from well data

Utilizing well data for architectural characterization is the most commonly used method in sedimentary research (He *et al.*, 2013; Kulga *et al.*, 2018; Chen *et al.*, 2023). Furthermore, horizontal wells provide abundant lateral information and enable the identification of architectural boundaries. Therefore, the integration of vertical and horizontal well data for architectural characterization has greatly reduced the uncertainty in predicting the scale and distribution of reservoir architectural elements (Fig. 2B). The specific steps are as follows: (1) Single-well architectural division is completed based on the interpretation conclusions of oilfield experts (Table 1); (2) After determining the sedimentary architecture of vertical wells, adjacent horizontal wells are used to characterize the lateral distribution of the architecture.

The application of quantitative geometric relationships can guide the characterization of sedimentary architecture (Leeder, 1973; Lorenz *et al.*, 1985; Wang *et al.*, 2017; Yue *et al.*, 2018, 2025b; Li *et al.*, 2023). The depth of distributary channels is obtained through compaction rate calculation and correction (Wang *et al.*, 2017). The empirical geometric relationship for the width of active channels is derived from Leeder (1973); the empirical geometric relationship for single channel belts is derived from Lorenz *et al.* (1985); and the empirical geometric relationship for point bar spans from Yue *et al.* (2018). In braided distributary channels, the length and width of braided bars as well as the number of braided bars in areas lacking well control are constrained by the empirical geometric relationship from Li *et al.* (2023). These quantitative geometric relationships serve as essential constraints on the predicted distribution and scale of sedimentary architecture.

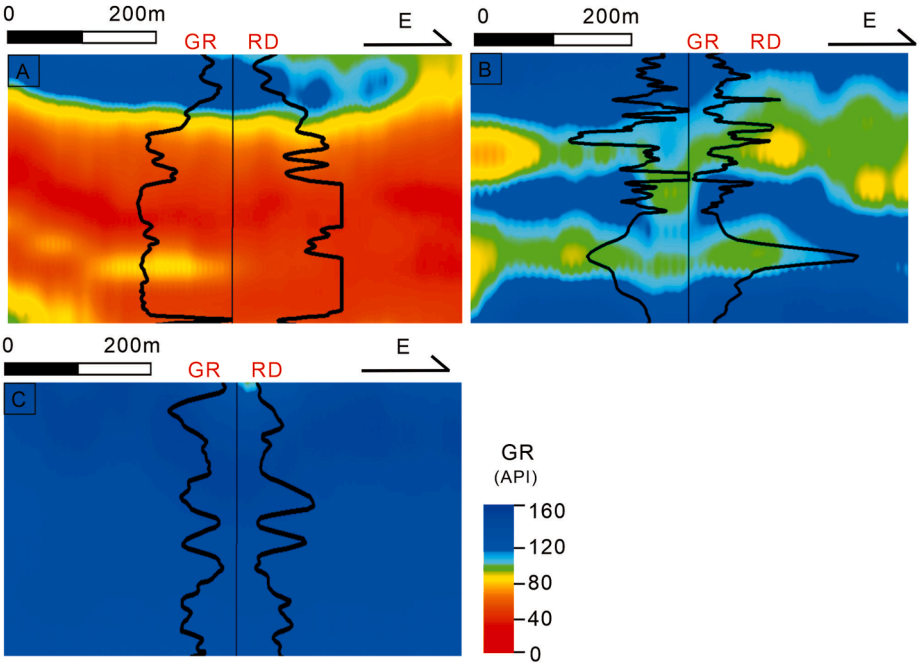

Fig. 3 Seismic inversion profile constrained by GR logging curves. A) The red inversion response (GR: 0—80 API) indicates distributary channels; B) The green inversion response (GR: 80—120 API) indicates overbanks; C) The blue inversion response (GR: 120—160 API) indicates interchannels. RD: Deep investigate double lateral resistivity log.

Table 1 Identification criteria for the architectural elements in the Shihezi Formation H8 Member of the study area.

Architecture elements	GR/(API)	TG/(%)	Logging rock debris
Point bar	25~102 (61.2)	0.4—12 (3.02)	Coarse sandstone
Abandoned channel	43~95 (76.1)	0.07—12 (0.15)	Fine sandstone
Braided bar	25~82 (58.5)	0.4—12 (3.95)	Gravelly coarse sandstone, coarse sandstone
Braided channel	24~94 (78.8)	0.1—12 (0.19)	Fine sandstone, medium sandstone
Overbank	94~110 (104.3)	0.07—0.29 (0.16)	Siltstone, argillaceous siltstone
Interchannel	110~162 (128.4)	0.07—0.24 (0.12)	Mudstone, silty mudstone

TG: Total gas, %. 25—102(61.2) represents the maximum value and the minimum value with the averages given in parentheses.

3.4. Dynamic data validation

Dynamic data, such as gas reservoir pressure (Wang *et al.*, 2025), initial daily gas production (He *et al.*, 2013), and quantum dot tracer tests (Silva *et al.*, 2025), are commonly used to validate the results of sedimentary architecture characterization. Within the same architectural elements, the pressure and daily gas production of production wells decrease annually due to the high internal connectivity of sand bodies (Deng *et al.*, 2003). Therefore, the characterization of these architectural elements can be verified by comparing the pressure and initial daily gas production of production wells commissioned at different times (Fig. 4A). The QDT quantitatively characterizes the production contribution rate of each fracturing stage in horizontal wells by labeling gas and water in the reservoir (Gao *et al.*, 2018; Silva *et al.*, 2025). Given that the physical properties and gas-bearing capacity of point bars are superior to those of abandoned channels (Winkels *et al.*, 2022), QDT was employed to validate their characterization in this study (Fig. 4B). The QDT test was conducted over a 2-month period from May 28 to July 28.

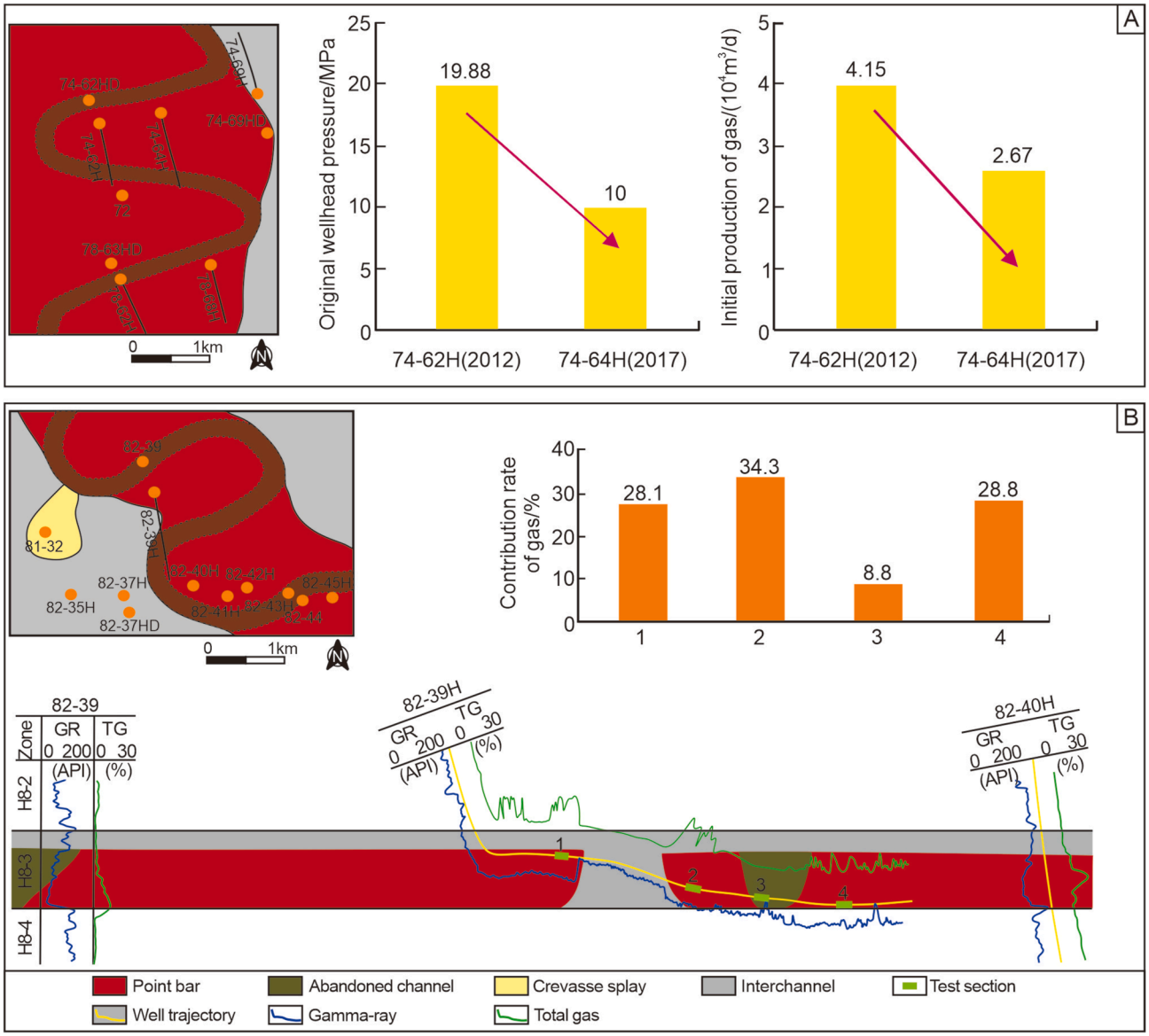

Fig. 4 Verification of architectural elements by using dynamic data. **A)** The original wellhead pressure decreased 9.88 MPa in Well 74—64H commissioned in 2017 compared with Well 74—62H commissioned in 2012 and the initial daily gas production decreased 1.48 × $10^4 m^3/d$, indicating high internal connectivity within the point bar; **B)** QDT production profile. The gas production contribution rates of fracturing stages 1, 2, and 4 (located within the point bar) are 28.1%, 34.3%, and 28.8%, respectively, whereas that of fracturing stage 3 (in the abandoned channel) is only 8.8%. This indicates that the gas production contribution rate of the abandoned channel is significantly lower than that of the point bar. GR: Gamma-ray, API (American Petroleum Institute units); TG: Total gas, %.

4. Results

4.1. Core characteristics of architecture elements

Braided and meandering distributary channels exhibit marked differences in lithology, sedimentary structures, and other characteristics (Fig. 5A, B and C).

The lithology of meandering distributary channels exhibits a downward-to-upward sequence of coarse sandstone, medium sandstone, fine sandstone, and minor argillaceous fine sandstone. The sedimentary structures are dominated by trough cross bedding, wedge-shaped cross bedding, and parallel bedding in an upward succession, respectively (Fig. 5A). The sand body thickness generally exceeds 3 m, with a predominantly positive grain-size rhythm. The interior of

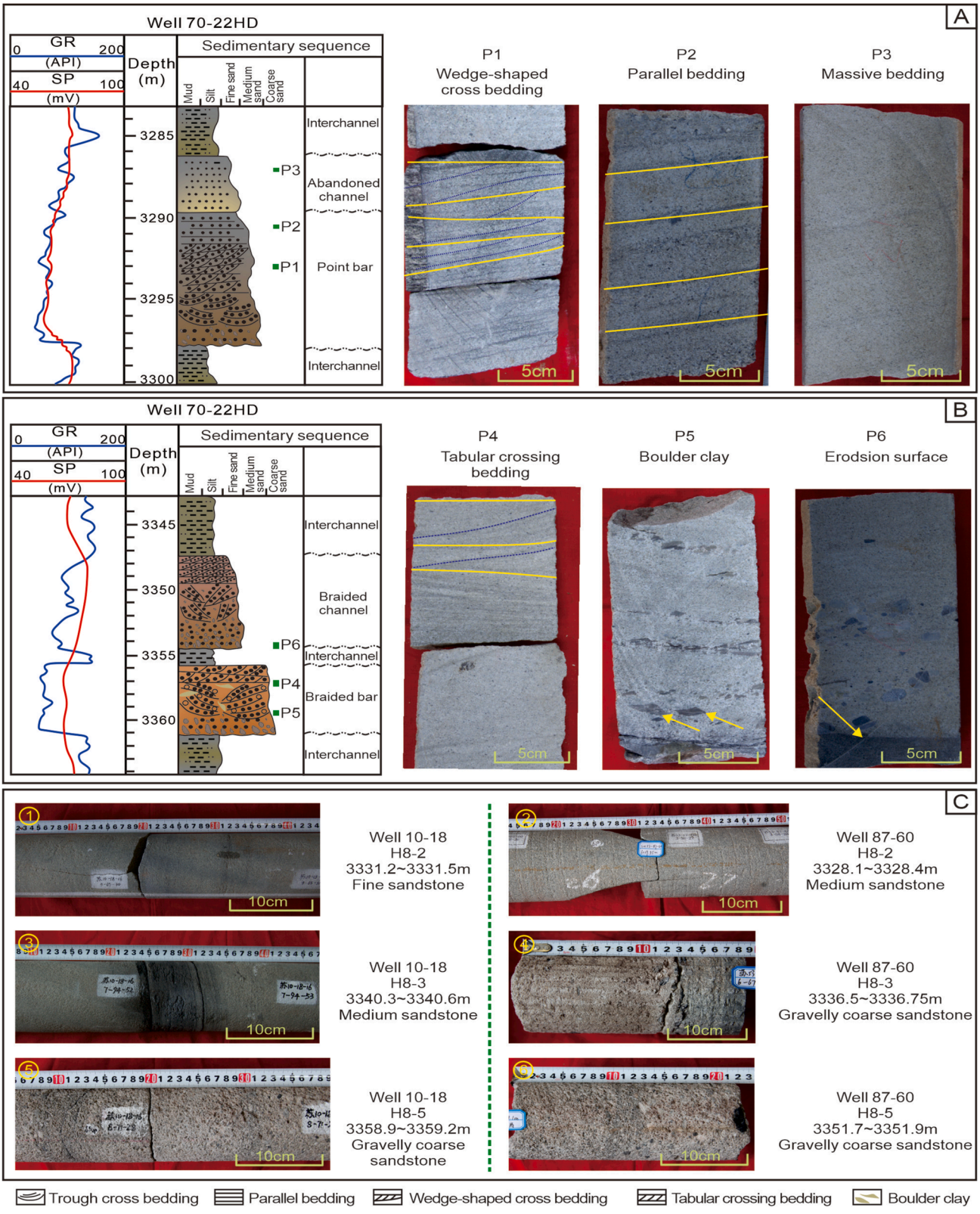

Fig. 5 Typical sedimentary sequences and core photographs of distributary channels in the H8 Member of the Shihezi Formation. **A)** Meandering distributary channels; **B)** Braided distributary channels; **C)** Core photographs of Wells 10—18 and 87—60 demonstrating the lateral facies changes among braided-dominated, transitional, and meandering-dominated zones. ① and ②: Core photographs of meandering distributary channel; ③ and ④: Core photographs of braided-meandering transitional distributary channel; ⑤ and ⑥: Core photographs of braided distributary channel.

meandering distributary channels can be further subdivided into point bars and abandoned channels, where the point bar sand bodies are thicker and coarser-grained than those in abandoned channels.

Vertically, braided distributary channels consist of gravelly coarse sandstone at the base, overlain by medium and fine sandstone. Trough and tabular cross-bedding are prevalent, with distinct erosion surfaces at the channel base indicative of strong hydrodynamic conditions (Fig. 5B). Sand bodies are predominantly homogeneous in rhythm and usually thicker than 3.5 m. Further internal division reveals braided bars and braided channels, where braided bar sand bodies are characterized by greater thickness and coarser grain size compared to braided channel sand bodies.

Overbank deposits can be subdivided into natural levees and crevasse splays. The lithology of natural levees consists of argillaceous siltstone, siltstone, and fine sandstone. The sand body thickness is generally less than 2 m, without obvious rhythmicity. The lithology of crevasse splays includes medium sandstone and fine sandstone; the sand body thickness ranges from 2 to 3 m (Table 2).

The lithology of interchannel is dominated by mudstone and silty mudstone, in which carbonaceous laminae and plant stem-leaf fossils are preserved. Sedimentary structures are mainly massive bedding, with wavy bedding occasionally observed (Table 2).

4.2. Architecture distribution of braided-meandering transitional delta

Following the forward architectural characterization method detailed in Sections 3.2, 3.3, and 3.4, the spatial distribution of architectural elements was identified. The meandering river delta plain subfacies is well developed in H8-2 zone (Fig. 6A). The meandering distributary channels strike nearly in the northeast-southwest direction, with a total of five channels identified. These channels exhibit a strip-shaped distribution pattern, with widths ranging from 1000 to 3000 m and an average width of approximately 1750 m. Internally, the point bars within the meandering distributary channels span 700—2750 m, with a mean span of about 2120 m. In contrast, the abandoned channels have widths varying from 450 to 510 m, with an average width of roughly 475 m.

The braided-meandering transitional delta plain subfacies is well developed in H8-3 zone (Fig. 6B). The distributary channels in this zone strike nearly north-south. The meandering distributary channels are developed in the mid-left part of the study area and situated between two braided distributary channels. The width of the meandering distributary channel is approximately 1820 m. In comparison, the braided distributary channels exhibit a banded or wide-banded distribution pattern, with a total of five distributary channels identified. Their widths range from 1050 to 3200 m, with an average width of about 2100 m.

The braided river delta plain subfacies is well developed in H8-5 zone (Fig. 6C). The braided distributary channels strike nearly north-south, with a total of eight channels identified. These channels exhibit a laterally connected sheet-like distribution pattern, which reflects the sedimentary characteristics of lateral migration of braided distributary channels. Their widths range from 1000 to 4100 m, with an average width of approximately 2850 m.

Distinct differences exist in the structural characteristics of different types of distributary channel sand bodies. The meandering distributary channel sand bodies are relatively thin and dominated by isolated vertical distribution, whereas the braided distributary channel sand bodies are thicker and primarily characterized by vertically incised and

Table 2 Characteristics of different architectural elements in the H8 Member of the study area.

Architectural elements		Lithology	Sedimentary structure	Thickness of the sandstone
Distributary channels	Meandering channel	Coarse sandstone	Trough cross bedding	>3 m
		Medium sandstone	Wedge-shaped cross bedding	
		Fine sandstone	Parallel bedding	
	Braided channel	Gravelly coarse sandstone	Erosion surface	>3.5 m
		Medium sandstone	Trough cross bedding	
		Fine sandstone	Tabular crossing bedding	
Overbank	Natural levee	Argillaceous siltstone	Wavy bedding	<2 m
		Siltstone	Parallel bedding	
		Fine sandstone		
	Crevasse splay	Fine sandstone	Wavy bedding	2~3 m
		Gravel medium sandstone	Parallel bedding	
Interchannel		Mudstone	Massive bedding	/
		Silty mudstone	Wavy bedding	

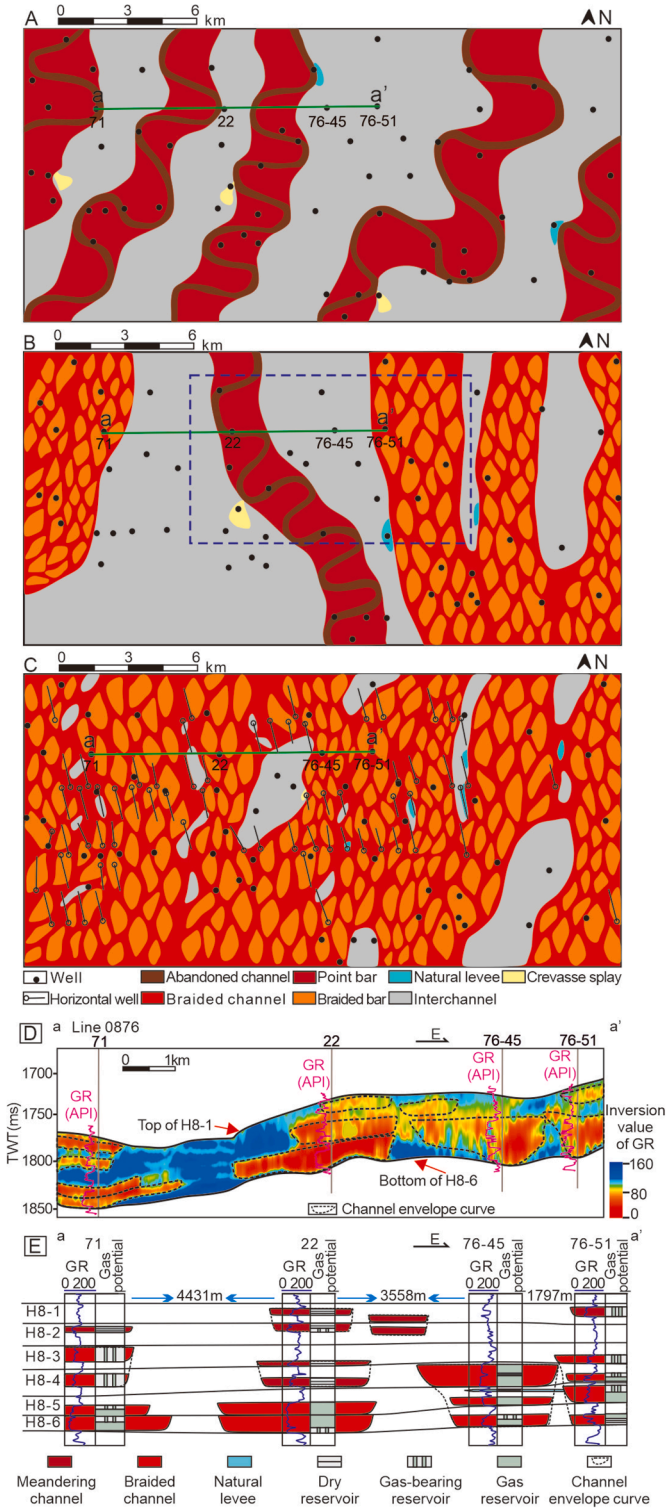

Fig. 6 **A)** Distribution of architectural elements of the meandering delta plain in H8-2 zone; **B)** Distribution of architectural elements of the braided-meandering transition delta plain in H8-3 zone; **C)** Distribution of architectural elements of the braided delta plain in H8-5 zone; **D)** The seismic inversion of profile aa' constrained by GR logging curves provided critical supplementary evidence for validating the lateral facies interpretation in Fig. 6A—C. Areas with lower values (represented by red and yellow) were defined as distributary channels, whereas areas with relatively higher values (represented by blue) were identified as interchannels; **E)** The distribution of distributary channel sand bodies of profile aa'.

superimposed distribution patterns (Fig. 6D and E). Within the H8-3 and H8-4 zones, the thickness of the intermediate meandering distributary channel sand bodies is significantly thinner than those of the adjacent braided distributary channel sand bodies (Fig. 6D and E), which further indicates the development of braided-meandering transitional distributary channels in these two zones.

5. Discussion

5.1. Evidence of the braided-meandering transition delta

5.1.1. The sinuosity index and rhythmic characteristics of distributary channel sand bodies

Schumm (1963) outlined methods for calculating river width-to-depth (W/D) ratios (Equation (1)) and channel sinuosity index (Equation (2)) based on bed-material grain size. The threshold sinuosity index of 1.3 proposed by Li *et al.* (2017) serves as the demarcation criterion for braided and meandering channels. The sinuosity index of distributary channels in braided-meandering transitional deltas ranges from 1.14 to 1.4, which is consistent with our architectural characterization results (Fig. 7A). This value differs from the threshold of 1.15 for distributary channels obtained by Yang *et al.* (2024) in the shallow-water delta plain of the Huagang Formation, Xihu Sag, East China Sea. This discrepancy may be attributed to variations in hydrodynamic conditions and sediment supply between the two basins. Therefore, for deltas in different regions, it is necessary to statistically analyze reasonable threshold values to distinguish between braided distributary channels and meandering distributary channels.

$$F = 255M^{-1.08};\ F, \text{Width} - \text{to} - \text{depth ratio};\ M, \text{The content of silt and clay}, \% \quad \text{(Equation 1)}$$

$$P = 0.94M^{-1.080.25};\ P, \text{Sinuosity index} \quad \text{(Equation 2)}$$

During the transition from braided river deltas to meandering rivers deltas, the proportion of sand bodies with a positive rhythm gradually increases, whereas the proportion of those with a homogeneous rhythm exhibits a decreasing trend (Fig. 7B). The specific statistical data regarding the proportion of different sedimentary rhythm types in each zone of the H8 Member are listed in Table 3. Braided river deltas typically exhibit stronger hydrodynamic conditions and more sufficient sediment supply, which accounts for the observed variation in the rhythm of sand bodies (García-García *et al.*, 2011; Celis *et al.*, 2021; Winkels *et al.*, 2022). In fluvial systems, sand bodies of meandering rivers predominantly exhibit by a positive rhythm, whereas those of braided rivers are dominated by a homogeneous one (Jorgensen, 1990; Wang *et al.*, 2017; Li *et al.*, 2023). The sedimentary characteristics of distributary channels on the delta plain are analogous to those of fluvial deposits, which also accounts for this sand body rhythmic pattern.

5.1.2. Comparison of architectural characterization and modern analogue

Abundant modern sedimentary analogs have documented the transition and coexistence of braided and meandering patterns in fluvial systems (La Croix *et al.*, 2019). Friend *et al.* (1993)measured and analyzed three rivers in India using satellite imagery, describing cases where braided rivers, meandering rivers, and their transitional types coexist in modern depositional settings. Similarly, Bridge and Tye (2000) further demonstrated that braided, meandering, and transitional channels can develop simultaneously within a single river system.

Satellite imagery also reveals the occurrence of braided-meandering transitions and coexistence on delta plains, such as a delta developed in the Qinghai Lake, China (Fig. 8A and B). A braided distributary channel with a sinuosity index of 1.27 and a channel width ranging from 305 to 412 m develops on the right side, whereas a meandering distributary channel with a sinuosity index of 1.38 and a channel width of 166—291 m occurs on the left side (Fig. 8C). Sedimentary architectural analysis of the study area reveals that within the braided-meandering transitional delta, a braided distributary channel exhibits a sinuosity index of 1.19 and a width ranging from 1600 to 2000 m, whereas a meandering distributary channel has a sinuosity index of 1.33 and a width of 945—1720 m (Fig. 8D). Based on the standard sinuosity ranges for global fluvial systems summarized by Friend and Sinha (1993) (1.0—1.35 for braided channels and 1.35—1.8 for meandering channels), the values calculated in this study (1.27 for braided channels and 1.38 for meandering channels) fall well within the globally accepted ranges. A quantitative comparison of the key sedimentary architecture parameters among the study area, the Qinghai Lake, and the Niger

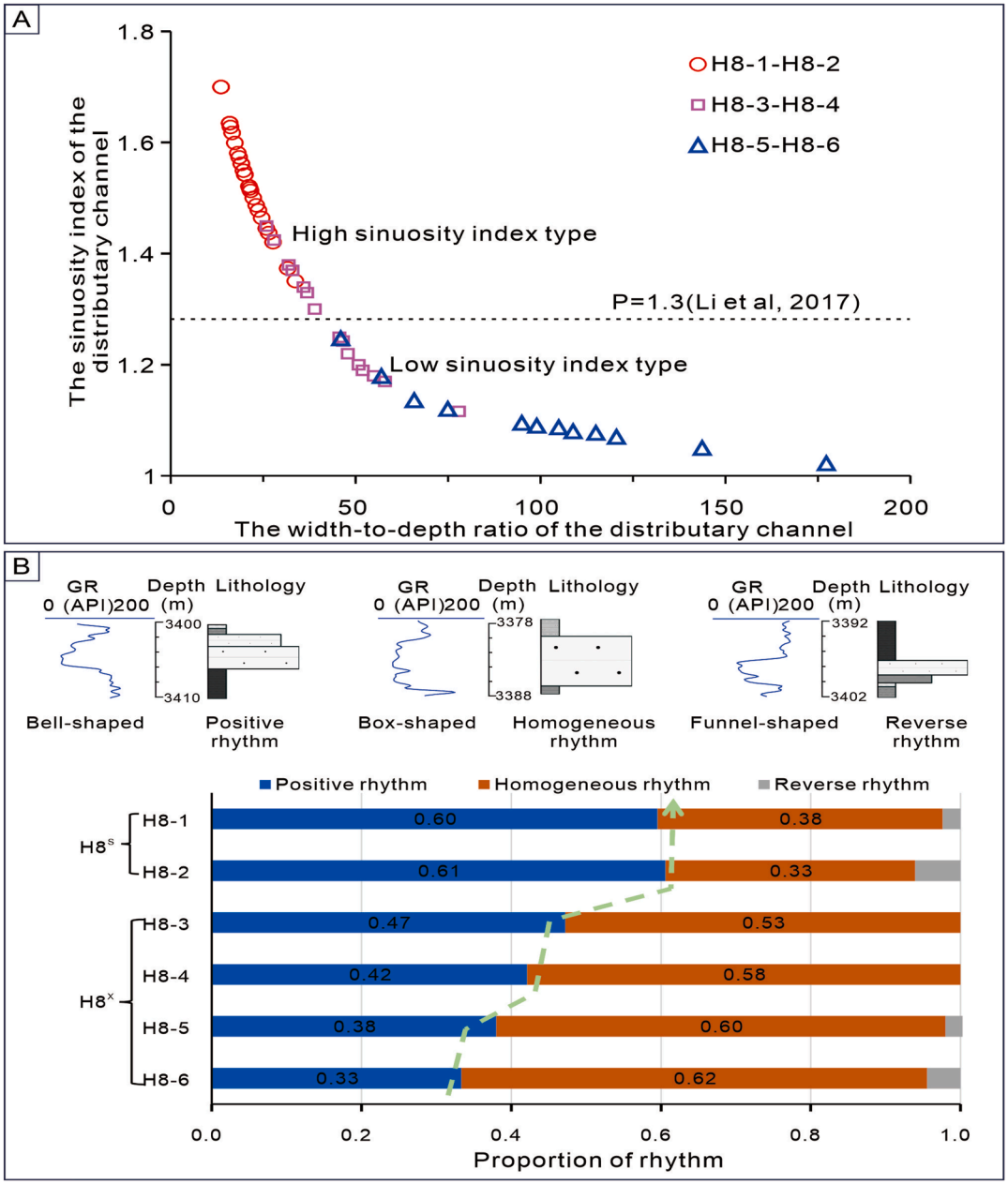

Fig. 7 **A)** Diagram of sinuosity index and width-to-depth ratio of distributary channels in the H8 Member of the Shihezi Formation.; **B)** Different logging curve shapes and sand body rhythm characteristics in the H8 Member of the Shihezi Formation and the rhythmic proportion of different sand bodies within different zones. The green arrow indicates an upward increase in the proportion of positive rhythms and a corresponding decrease in homogeneous rhythms from bottom to top.

Table 3 Proportion of different sedimentary rhythm types in various zones of the H8 Member.

Zone rhythm type	H8-1	H8-2	H8-3	H8-4	H8-5	H8-6
Positive rhythm	0.6	0.61	0.47	0.42	0.38	0.33
Homogeneous rhythm	0.38	0.33	0.53	0.58	0.6	0.62
Reverse rhythm	0.02	0.06	0	0	0.02	0.05

Delta is summarized in Table 4. The differences in the quantitative parameters of distributary channels may be attributed to variations in sedimentary conditions, coupled with limited seismic resolution and uncertainties in the BPNN inversion results, which propagate to architectural interpretations.

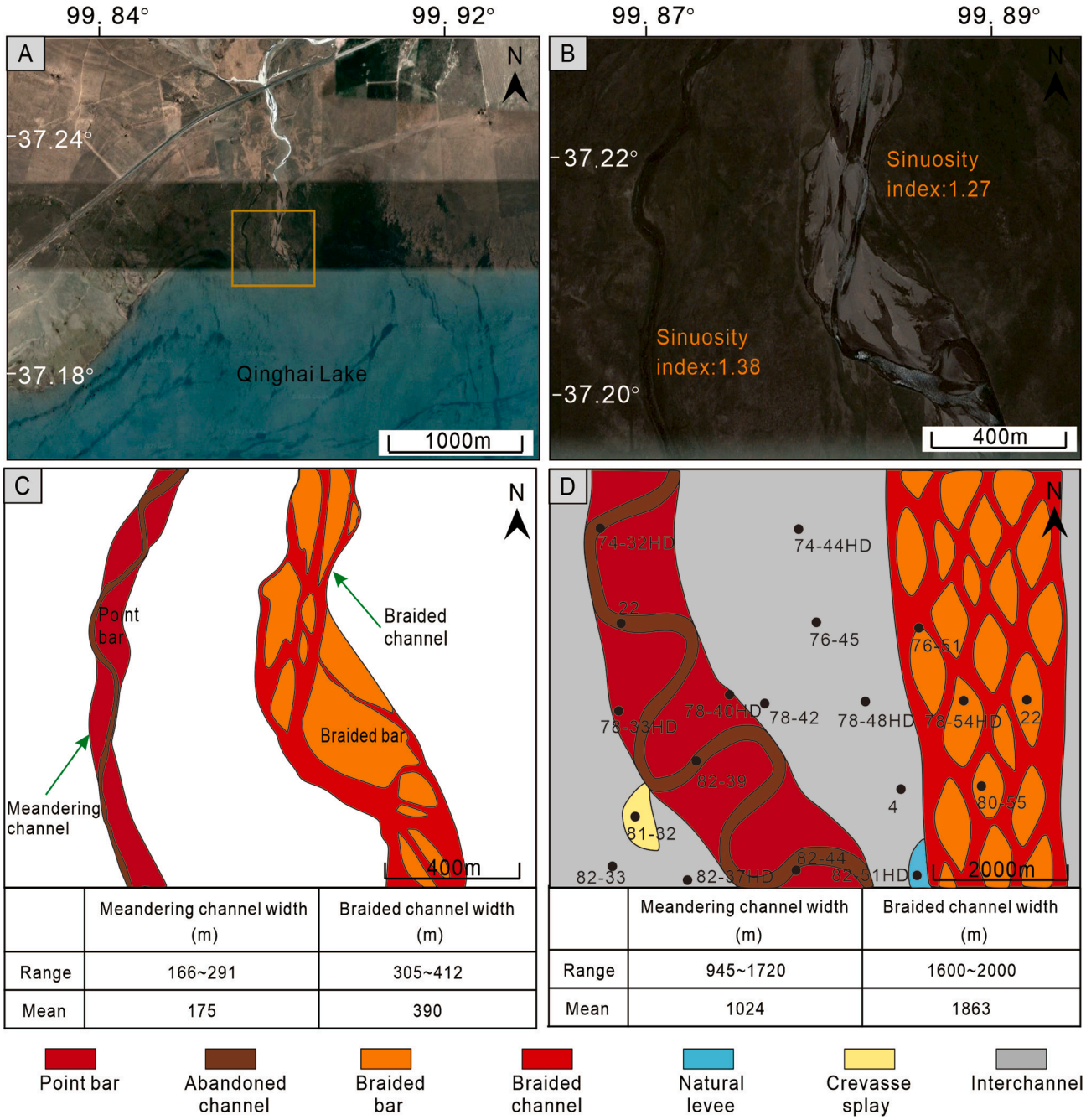

	Meandering channel width (m)	Braided channel width (m)
Range	166~291	305~412
Mean	175	390

	Meandering channel width (m)	Braided channel width (m)
Range	945~1720	1600~2000
Mean	1024	1863

Fig. 8 **A)** Modern sedimentary example of coexistence and transformation of braided-meandering distributary channels in the Qinghai Lake; **B)** The enlarged view within the yellow bounding box in Fig. 8A reveals some details of the coexistence and transformation of braided-meandering distributary channels; **C)** Planar distribution of distributary channel and their internal architectural elements of Fig. 8B; **D)** An example of coexistence and transformation of braided-meandering distributary channels in the study area, with the scope corresponding to the blue box in Fig. 6B.

5.2. Evolution pattern of the sedimentary architecture of the braided-meandering transitional delta

Base-level fluctuations were identified and quantified using Gamma-ray (GR) log trends. Medium-term base-level cycles are characterized by amplitudes of 15—20 m and durations of 0.5—1 Ma, while long—term cycles show larger amplitudes (40—60 m) and longer durations (1.5—2 Ma) (Tao *et al.*, 2025). According to the characteristics of architectural elements and changes in the base level, we established sedimentary

Table 4 Comparison of quantitative sedimentary architecture parameters among the braided-meandering transitional delta in the Ordos Basin, the Qinghai Lake and the Niger Delta.

	Range of distributary channel widths (m)		Mean sinuosity index	
	Braided	Meandering	Braided	Meandering
The Ordos Basin (this study)	1450~2100	850~1850	1.16	1.51
The Qinghai Lake (satellite imagery)	166~291	305~412	1.27	1.38
The Niger Delta (Reijers, 2011; Ignatius *et al.*, 2025)	630~1510	320~1260	1.29	2.13

patterns for different evolutionary stages of the braided-meandering transitional delta. With the gradual rise of the base level, the braided river delta evolves into a braided-meandering transitional delta, and finally transitions into a meandering river delta at a high base level (Fig. 9A, B, and C). Changes in the base level reflect the relative changes in accommodation space and sediment flux (He *et al.*, 2014). At a low base level, abundant provenance supply and high hydrodynamic energy of distributary channels, together with bed load-dominated sediment composition and intense scouring-erosion processes (Schumm, 1981), drive the development of braided distributary channels (Fig. 9A). With the rise of the base level, accommodation space increases while channel energy decreases, which enhances lateral erosion and further triggers the transformation of some braided channels into meandering ones (Fig. 9B). Thus, sediment flux to the lake was reduced, and the grain size was significantly refined (Zheng et al., 2000), which contributes to the formation of meandering distributary channels (Fig. 9C).

The braided-meandering delta patterns established in this study can be partially compared with the data reported in the literature. The patterns established in this study are analogous to those proposed by Yang *et al.* (2024) for the shallow-water delta plain of the Huagang Formation in the Xihu Sag, East China Sea, since both study areas are characterized by similar gentle tectonic settings and rising base-level conditions. Pennington *et al.* (2017) noted that with the rise of the base level, the Holocene Nile Delta was dominated by meandering river deltas. This phenomenon may be attributed to factors such as the distant provenance and fine-grained sediment composition of the delta (Hennekam *et al.*, 2015; Pennington *et al.*, 2017). For deltas formed by rivers draining into the ocean, such as the Bengal Delta (Akter *et al.*, 2016), the effects of waves and tides may increase sediment resuspension (Zhang *et al.*, 2020), thereby further complicating this braided-meandering transition process. Therefore, it is essential to acknowledge that the braided-meandering transition of deltas is also influenced by tectonic movements (Zeng *et al.*, 2017; Yang *et al.*, 2024), climatic conditions (Tang *et al.*, 2016; Zhao *et al.*, 2019), and vegetation development (Winkels *et al.*, 2022) and other relevant factors.

The braided-meandering transitional delta has not garnered sufficient research attention, consequently, its conceptual pattern has yet to be fully applied to the interpretation of ancient deltaic systems. The evolutionary pattern of braided-meandering transitional deltas established in this study may serve as a valuable supplement to the field of delta sedimentology, providing new insights into the characterization of ancient deltas (Zeng *et al.*, 2017; Yang *et al.*, 2024).

5.3. *Indicative meaning of the sedimentary architecture of the braided-meandering transitional delta*

The braided-meandering transition in deltas has not attracted sufficient attention from geologists. The evolution patterns of braided-meandering deltas are not only critical for the architectural distribution of ancient deltas, but also highly valuable for predicting the spatial distribution of high-quality reservoirs in tight oil and gas systems.

Some studies have confirmed that braided-river deltas are generally characterized by coarser grain sizes and better porosity and permeability than meandering-river deltas (Zhu *et al.*, 2017; Winkels *et al.*, 2022). In tight-gas reservoirs characterized by underdeveloped fault systems and relatively stable tectonic settings—such as the Sulige Gas Field—the dominant sedimentary architecture exerts a primary control on the distribution of high-quality reservoirs and thereby affects gas productivity (Yang *et al.*, 2008; Wu *et al.*, 2022). Sand bodies of the stacked braided distributary channels are characterized by greater thickness, and their gas-bearing properties are superior to those of the isolated sand bodies of meandering distributary channels (Fig. 10A and B). Wells 82—42H and 78—36H, which drilled through more braided bar sand bodies, exhibit the highest initial daily gas production and average daily gas production (Fig. 10C and D). Therefore, the establishment of the braided-meandering transitional delta patterns is of considerable significance for enhancing

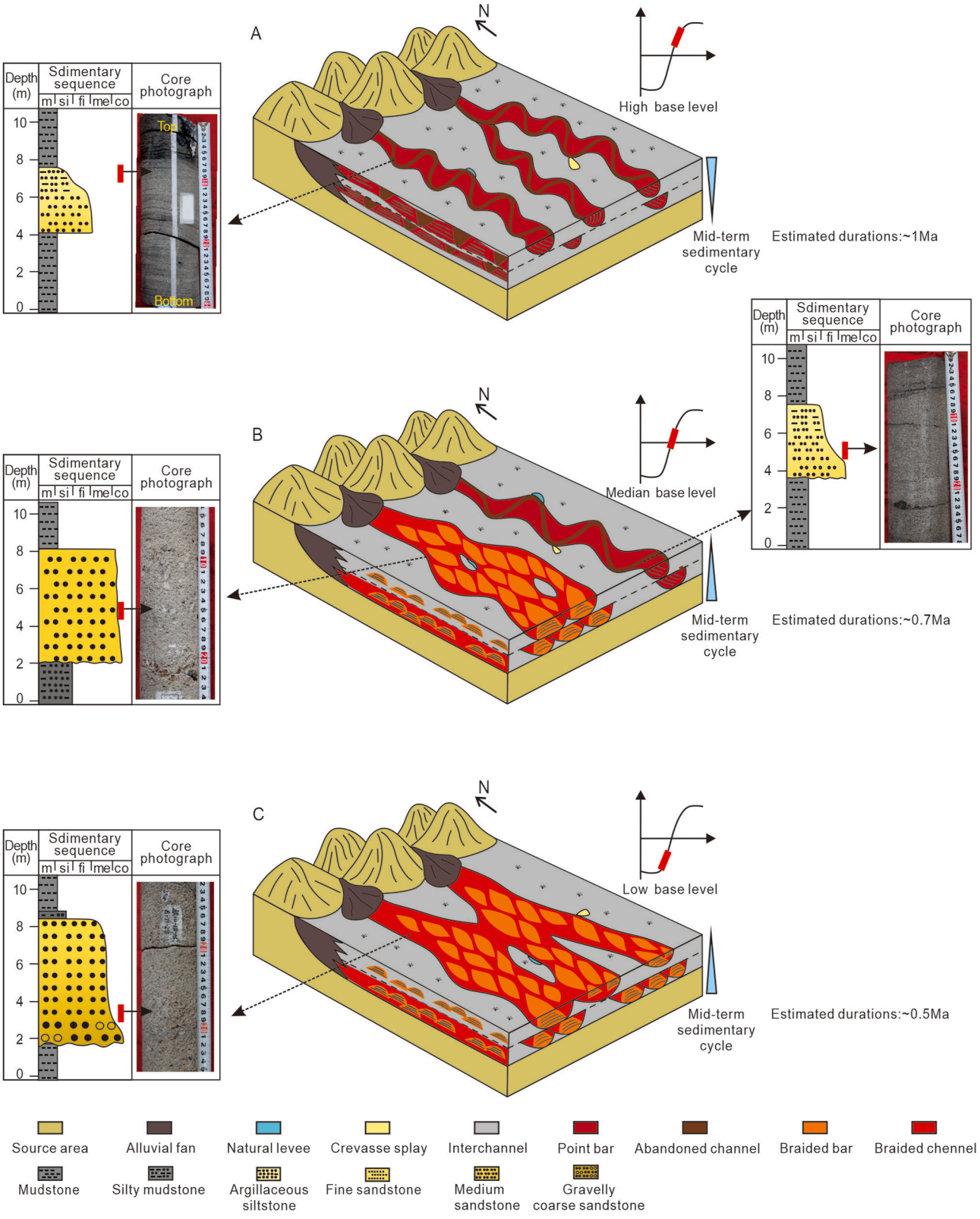

Fig. 9 **A)** Sedimentary pattern, sedimentary sequence, and typical core photographs of the meandering river delta in the H8 Member of the study area; **B)** Sedimentary pattern, sedimentary sequence, and typical core photographs of the braided-meandering transitional delta in the H8 Member of the study area; **C)** Sedimentary pattern, sedimentary sequence, and typical core photographs of the braided river delta in the H8 Member of the study area. Upward blue vertical triangles represent mid-term base-level rises, while downward blue vertical triangles represent mid-term base-level falls. Low base level: an estimated duration of ~0.5 Ma; Medium base level: ~0.7 Ma; High base level: ~1 Ma.5.3.

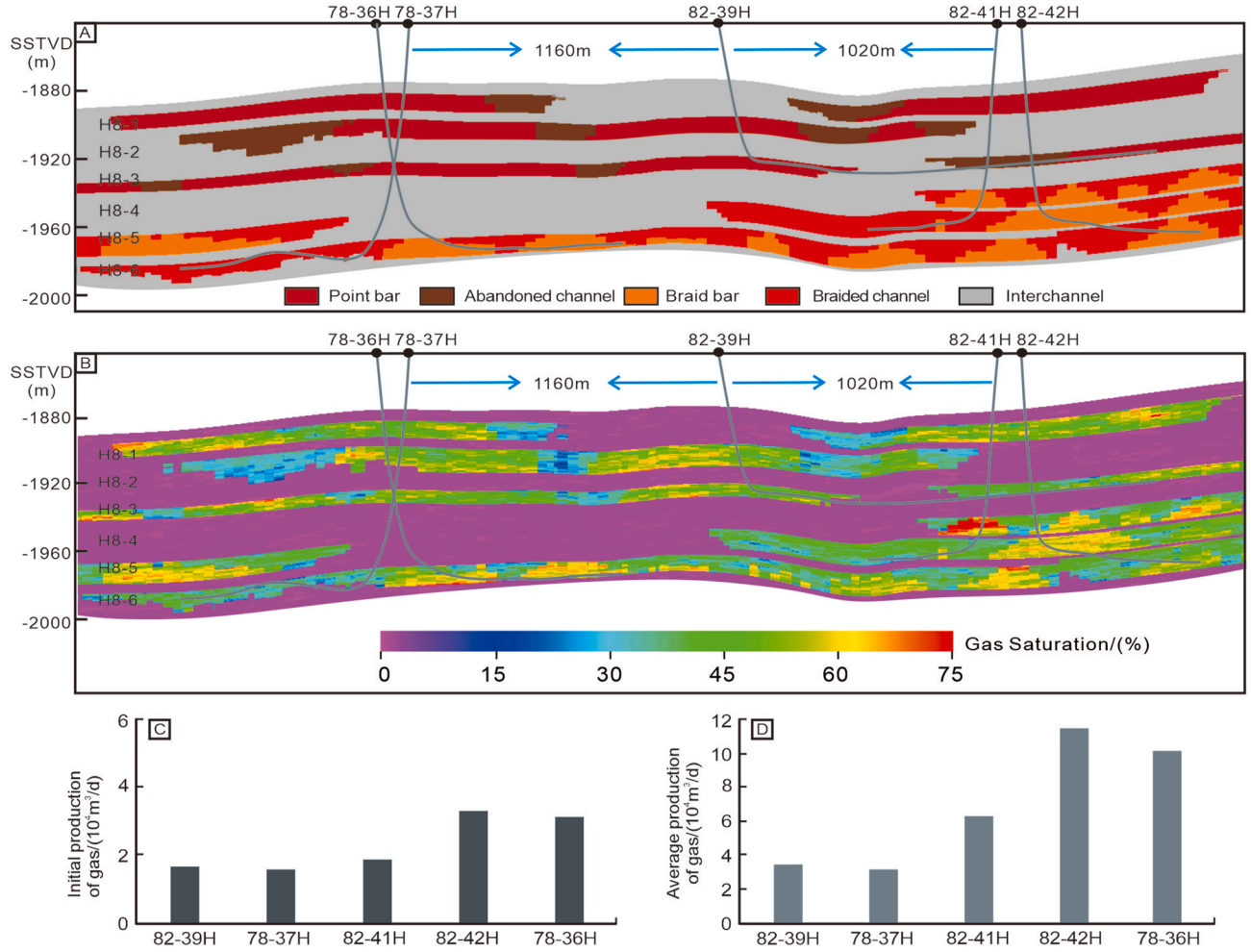

Fig. 10 **A)** The profile of architecture model; **B)** The profile of gas saturation, corresponding to Fig. 10A; **C)** The initial gas production of horizontal wells in Fig. 10A; **D)** The average gas production of horizontal wells in Fig. 10A. SSTVD: Sub-surface ture vertical depth.

exploration success rates and guiding horizontal-well deployment strategies in analogous oil and gas fields.

5.4. Limitations

The study area is covered by thick loess, which has resulted in generally suboptimal quality of the seismic data. Due to this data limitation and the inherent characteristics of seismic inversion, the BPNN inversion results exhibit significant uncertainties in the detailed imaging of thin, isolated meandering distributary channel sands (Duan *et al.*, 2025). Consequently, the seismic inversion results only provide constraints for the interpretation of composite distributary channels. Nevertheless, the area benefits from a dense well network, particularly with closely spaced horizontal wells (Fig. 1C). Integrating the inversion results with the dense well data effectively reduces the uncertainty in sandbody prediction. Therefore, the evolutionary patterns of the braided-meandering transitional delta proposed in this study demonstrate considerable reliability.

6. Conclusions

1) This study applied an integrated approach combining seismic inversion, well logging, and dynamic data to characterize the sedimentary architecture in the H8 Member. Within the study area, the delta exhibits vertical braided-meandering transition and the coexistence of local single zones.
2) In the H8 Member of the study area, base-level fluctuation is identified as the primary control on the transformation of braided-meandering

transitional deltas. As the base level rises progressively, the braided-river delta evolves into the braided-meandering transitional delta and ultimately develops into the meandering-river delta.

3) From an applied perspective, the braided distributary channel sandbodies in the H8 Member exhibit superior reservoir quality and gas-bearing properties, which could provide guidance for enhancing oil and gas recovery efficiency in the study area. Although this study still has certain limitations, continuous in-depth research will advance the understanding of deltaic systems.

CRediT authorship contribution statement

Ming-Qiang Li: Writing — original draft, Visualization, Investigation, Formal analysis, Data curation, Conceptualization. **Da-Li Yue:** Writing — review & editing, Project administration, Methodology, Funding acquisition, Conceptualization. **Qin-Xi Tang:** Supervision, Resources, Project administration, Funding acquisition. **Wu-Rong Wang:** Validation, Supervision, Formal analysis, Conceptualization. **Qi Wang:** Resources, Project administration. **Jia-Rui Zhang:** Visualization, Software, Formal analysis, Data curation. **Wei Li:** Writing — review & editing, Supervision, Funding acquisition. **Zi-Mo Xu:** Formal analysis, Data curation. **Ying-Bo Yuan:** Visualization, Formal analysis.

Declaration of interests

The authors declare that they have no known competing financial interests or personal relationships that could have appeared to influence the work reported in this paper.

Acknowledgements

This research was financially supported by the National Science and Technology Major Project of China (Nos. 2025ZD1404304, 2024ZD1406601), National Natural Science Foundation Project of China (Nos. 42202109, 42272186, 42302128, 42472179). The authors greatly appreciate Sulige Gas Filed Branch, CNPC Greatwall Drilling Company, for their support in permission to publish the results.

References

Akter, J., Sarker, M.H., Popescu, I., Roelvink, D., 2016. Evolution of the Bengal Delta and its prevailing processes. *Journal of Coastal Research*, 32(5), 1212—1226.

Bridge, J.S., Tye, R.S., 2000. Interpreting the dimensions of ancient fluvial channel bars, channels, and channel belts from wireline-logs and cores. *AAPG Bulletin*, 84(8), 1205—1228.

Bridge, J.S., 2003. *Rivers and Floodplains*. Blackwell Publishing, Oxford, UK, pp. 491—492.

Cao, H., Zhao, Y., Chen, H.C., Zhang, L.L., Xian, C.G., Yang, J.D., Liu, L., 2025. Integrating well logs, 3D seismic, and earthquake data for comprehensive prediction of 3D in-situ stress orientations: A case study from the Weiyuan area in the Sichuan Basin, China. *Petroleum Science*, 22(1), 210—221.

Celis, S.A., Rodríguez-Tovar, F.J., Giraldo-Villegas, C.A., Pardo-Trujillo, A., 2021. Evolution of a fluvial-dominated delta during the Oligocene of the Colombian Caribbean: Sedimentological and ichnological signatures in well-cores. *Journal of South American Earth Sciences*, 111, 103440.

Chapkanski, S., Brocard, G., Lavigne, F., Afrizal, T., Meilianda, E., Ismail, N., Majewski, J., Daly, P., Horton, B., Switzer, A., Steuer, A., Siemon, B., Darusman, D., Virmoux, C., Goiran, J.P., 2025. Mid-to-late Holocene fluvial and coastal evolution in the Aceh River delta, Sumatra: effects of sea-level change, sediment supply, wave climate, tectonics and tsunamis. *Quaternary Science Advances*, 19, 100290.

Chen, Q., Liu, Y.M., Feng, Z., Hou, J.G., Bao, L., Liang, Z., 2023. The architecture characterization of braided river reservoirs in the presence of horizontal wells—An application in a tight gas reservoir in the North Ordos Basin, China. *Energies*, 16(20), 7092.

Chen, Y., Li, J.G., Chen, L.L., Zhao, H.L., 2025. Mesozoic multi-direction collision tectonic evolution of the Ordos Basin, China: Insights from the detrital zircon and apatite (U-Th)/He analyses. *China Geology*, 8(1), 141—158.

Chu, R.J., Wu, H.C., Fang, Q., Huang, W.T., Liu, D.Y., Zhu, R.K., Zhang, S.H., Yang, T.S., Wang, C.S., 2023. Nonlinear responses to orbital forcing inferred from an analysis of lacustrine-delta sequences spanning the Middle Triassic (Ladinian) hyperthermal episode in the Ordos Basin, China. *Palaeogeography, Palaeoclimatology, Palaeoecology*, 628, 111763.

Coleman, J.M., Wright, L.D., 1975. *Modern River Deltas: Variability of Processes and Sand Bodies*. Houston Geological Society, pp. 99—149.

Côrte, G., Dramsch, J., Amini, H., MacBeth, C., 2020. Deep neural network application for 4D seismic inversion to changes in pressure and saturation: Optimizing the use of synthetic training datasets. *Geophysical Prospecting*, 68(7), 2164—2185.

Deng, Y.E., Liu, S.G., Ma, C.J., 2003. Aggregate analysis method of continuity of formation between wells. *Fault-Block Oil Gas Field*, 10(5), 50—53.

Duan, P.R., Huang, Y., Li, F., Chen, J., Ma, Y.L., Gu, B.L., 2025. Mega-merge processing with attenuation compensation from 3D pre-stack seismic data: A case study from a loess plateau area, southwest of Ordos Basin, China. *Journal of Applied Geophysics*, 236, 105669.

Ehsan, M., Manzoor, U., Chen, R.J., Hussain, M., Abdelrahman, K., Radwan, A.E., Ullah, J., Iftikhar, M.K., Arshad, F., 2025. Pore pressure prediction based on conventional well logs and seismic data using an advanced machine learning approach. *Journal of Rock Mechanics and Geotechnical Engineering*, 17(5), 2727—2740.

Fawad, N., Liu, T.Y., Fan, D.D., Ahmed, Q.A., Kamran, M., Ayub, G., 2023. Sequence stratigraphic divisions and correlation of the middle sub-member of Eocene Shahejie Formation in the Bonan Sag of Bohai Bay Basin (China): Implication for facies and reservoir heterogeneities. *Geoenergy Science and Engineering*, 225, 211622.

Friend, P.F., Sinha, R., 1993. Braiding and meandering parameters. *Geological Society, London, Special Publications*, 75(1), 105—111.

Fu, J.H., Fan, L.Y., Liu, X.S., Huang, D.J., 2018. Gas accumulation conditions and key technologies for exploration & development of Sulige gasfield. *Petroleum Research*, 3(2), 91—109.

Galloway, W.E., 1975. Process framework for describing the morphologic and stratigraphic evolution of deltaic depositional systems. In: Broussard, M. (Ed.), *Deltas: Models for Exploration*. Houston Geological Society, Houston, pp. 87—98.

Gao, X.J., Xu, W.W., Yu, Y.C., Li, Y.R., Li, L., 2018. Intelligent chemical tracer technology and its application to reservoir surveillance. *Advances in Earth Science*, 33(5), 532—544.

García-García, F., Corbí, H., Soria, J.M., Viseras, C., 2011. Architecture analysis of a river flood-dominated delta during an overall sea-level rise (early Pliocene, SE Spain). *Sedimentary Geology*, 237(1—2), 102—113.

Guo, Y.Q., Li, B.Q., Li, B., Li, W.H., Cao, H.X., Liao, Y., Wu, Z.Z., Fei, S.X., Zhang, Q., Chen, Q., Wang, R.G., Ma, Y., Yuan, Z., Li, Z.C., Fu, S., 2025. Sedimentary system and palaeogeographic evolution of Ordos Basin, northern China. *Journal of Palaeogeography*, 14(2), 501—534.

He, D.B., Jia, A.L., Ji, G., Wei, Y.S., Tang, H.F., 2013. Well type and pattern optimization technology for large scale tight sand gas, Sulige gas field, NW China. *Petroleum Exploration and Development*, 40(1), 84—95.

He, T.T., Li, S.L., Gao, X.J., Song, C., Zhou, X.M., He, D.X., 2014. Types and superposed patterns of distributary channels in a shallow lacustrine delta plain. *Journal of Palaeogeography*, 16(5), 597—604 (in Chinese with English abstract).

Hennekam, R., Donders, T.H., Zwiep, K., de Lange, G.J., 2015. Integral view of Holocene precipitation and vegetation changes in the Nile catchment area as inferred from its delta sediments. *Quaternary Science Reviews*, 130, 189—199.

Ignatius, A.A., Mode, A.W., Njoku, I.O., Okoro, E.M., 2025. Sequence stratigraphic and reservoir modeling of KOC Field onshore Niger Delta Basin: implication for mature oilfield revitalization. *Marine and Petroleum Geology*, 182, 107553.

Jia, A.L., Chen, F.X., Feng, N.C., Meng, D.W., Zheng, S., 2024. Model construction and implementation of Ordos Energy Super Basin, NW China. *Petroleum Exploration and Development*, 51(6), 1628—1640.

Jorgensen, D.W., 1990. *Adjustments of Alluvial River Morphology and Processes to Localized Active Tectonics*. Colorado State University, Fort Collins, Colorado, pp. 240—241.

Kulga, B., Artun, E., Ertekin, T., 2018. Characterization of tight-gas sand reservoirs from horizontal-well performance data using an inverse neural network. *Journal of Natural Gas Science and Engineering*, 59, 35—46.

La Croix, A.D., Dashtgard, S.E., MacEachern, J.A., 2019. Using a modern analogue to interpret depositional position in ancient fluvial-tidal channels: Example from the McMurray Formation, Canada. *Geoscience Frontiers*, 10(6), 2219—2238.

Leeder, M.R., 1973. Fluviatile fining-upwards cycles and the magnitude of palaeochannels. *Geological Magazine*, 110(3), 265—276.

Leila, M., Moscariello, A., 2018. Depositional and petrophysical controls on the volumes of hydrocarbons trapped in the Messinian reservoirs, onshore Nile Delta, Egypt. *Petroleum*, 4(3), 250—267.

Li, W., Colombera, L., Yue, D.L., Mountney, N.P., 2023. Controls on the morphology of braided rivers and braid bars: An empirical characterization of numerical models. *Sedimentology*, 70(1), 259—279.

Li, S.L., Yu, X.H., Jiang, T., Liang, X.R., Su, D.X., 2017. Meander-braided transition features and abandoned channel patterns in fluvial environment. *Acta Sedimentologica Sinica*, 35(1), 1—9 (in Chinese with English abstract).

Li, S.L., Ma, S.P., Zhou, L.W., Huang, X.D., Han, B., Li, H., 2022. Main influencing factors of braided-meander transition and coexistence characteristics and implications of ancient fluvial sedimentary environment reconstruction. *Earth Science*, 47(11), 3960—3976.

Liu, J.S., Zhang, G.J., Bai, J.P., Ding, W.L., Yang, H.M., Liu, Y., 2022. Quantitative prediction of the drilling azimuth of horizontal wells in fractured tight sandstone based on reservoir geomechanics in the Ordos Basin, central China. *Marine and Petroleum Geology*, 136, 105439.

Liu, K., Wang, R., Shi, W.Z., Zhang, W., Qi, R., Qin, S., Xu, L.T., 2020. Tectonic controls on Permian tight gas accumulation: Constrains from fluid inclusion and paleo-structure reconstruction in the Hangjinqi area, northern Ordos Basin, China. *Journal of Natural Gas Science and Engineering*, 83, 103616.

Lorenz, J.C., Heinze, D.M., Clark, J.A., Searls, C.A., 1985. Determination of widths of meander-belt sandstone reservoirs from vertical downhole data, Mesaverde Group, Piceance Creek Basin, Colorado. *AAPG Bulletin*, 69(5), 710—721.

McPherson, J.G., Shanmugam, G., Moiola, R.J., 1987. Fan-deltas and braid deltas: Varieties of coarse-grained deltas. *GSA Bulletin*, 99(3), 331—340.

Mousavi, S.M., Beroza, G.C., Mukerji, T., Rasht-Behesht, M., 2024. Applications of deep neural networks in exploration seismology: A technical survey. *Geophysics*, 89(1), WA95—WA115.

Moyano Paz, D., Richiano, S., Varela, A.N., Gómez Dacál, A.R., Poiré, D.G., 2020. Ichnological signatures from wave- and fluvial-dominated deltas: The La Anita Formation, Upper Cretaceous, Austral-Magallanes Basin, Patagonia. *Marine and Petroleum Geology*, 114, 104168.

Pang, J.G., Colombera, L., Mountney, N.P., Guo, J.A., Yang, K.W., Li, W.H., 2024. Mapping palaeoshorelines of river-dominated deltas in lacustrine ramp settings: Application of sedimentological analyses to the Triassic Yanchang Formation (Ordos Basin, China). *Marine and Petroleum Geology*, 164, 106797.

Pennington, B.T., Sturt, F., Wilson, P., Rowland, J., Brown, A.G., 2017. The fluvial evolution of the Holocene Nile Delta. *Quaternary Science Reviews*, 170(15), 212—231.

Postma, G., 1990. Depositional architecture and facies of river and fan deltas: a synthesis. In: Colella, A., Prior, D.B. (Eds.), *Coarse-grained Deltas*. International Association of Sedimentologists Special Publication, Blackwell, Oxford, pp. 13—27.

Reijers, T.J.A., 2011. Stratigraphy and sedimentology of the Niger Delta. *Geologos*, 17(3), 133—162.

Ricker, N., 1953. The form and laws of propagation of seismic wavelets. *Geophysics*, 18(1), 10—40.

Schumm, S.A., 1963. Sinuosity of alluvial rivers on the Great Plains. *Geological Society of America Bulletin*, 74(9), 1089—1100.

Schumm, S.A., 1981. *Evolution and response of the fluvial system, sedimentologic implications*, vol. 31. Society of Economic Paleontologists and Mineralogists, Special Publication, pp. 19—29.

She, G., Zhou, X.Y., Wang, J.B., 2013. Prediction of sand reservoir with multi-wavelet seismic trace decomposition and reconstruction. *Journal of Southwest Petroleum University (Science & Technology Edition)*, 35(1), 19—27.

Shehata, A.A., Sarhan, M.A., Abdel-Fattah, M.I., Assal, E.M., 2023. Sequence stratigraphic controls on the gas-reservoirs distribution and characterization along the Messinian Abu Madi incision, Nile Delta Basin. *Marine and Petroleum Geology*, 147, 105988.

Silva, C.F., Vasconcelos, K.C., Barros, A.F., Bernardo, V.B., Oliveira, L.F.A.M., Fonseca, E.J.S., Tonholo, J., Zanta, C.L.P.S., Duarte, J.L.S., Oliveira, L.M.T.M., 2025. Green carbon quantum dots applied as tracer for petroleum reservoir characterization. *Sustainable Materials and Technologies*, 43, e01274.

Syvitski, J.P.M., Kettner, A.J., Correggiari, A., Nelson, B.W., 2005. Distributary channels and their impact on sediment dispersal. *Marine Geology*, 222—223, 75—94.

Tang, W., Wang, Y.M., Zhao, Z.G., Zhong, M.H., Zhao, Y.N., Tian, J.H., Zou, M.J., 2016. A review of fluvial pattern transformation. *Geological Review*, 62(1), 138—152.

Tao, H., Cui, J.P., Sun, J.P., Ren, Z.L., Zhao, F.F., Su, S.H., Guo, W., Song, H.Y., 2025. Late Carboniferous to Permian paleoclimatic and tectono-sedimentary evolution of the central Ordos Basin, western north China Block. *Marine and Petroleum Geology*, 173, 107287.

Wang, H.F., Fan, T.E., Song, L.M., Hu, G.Y., Liang, X., Wang, S., Liu, X.N., 2017. Quantitative characterization study on sand body scale in high sinuosity meandering river. *Acta Sedimentologica Sinica*, 35(2), 279—289 (in Chinese with English abstract).

Wang, S.L., Yang, X.R., Lu, Y.Y., Su, P.D., Liu, D., Meng, L.J., Wang, Q., Li, L., Radwan, A.E., 2022. Densification mechanism of deep low-permeability sandstone reservoir in deltaic depositional setting and its implications for resource development: A case study of the Paleogene reservoirs in Gaoshangpu area of Nanpu sag, China. *Frontiers in Earth Science*, 10, 996167.

Wang, Z.C., Tian, L., Li, J.B., Li, P., Chai, X.L., Deng, X.J., Jiang, L.L., 2025. Reserve utilization evaluation model for tight gas well based on low-velocity non-Darcy seepage. *Journal of Natural Gas Geoscience*, 10(5), 331—341.

Winkels, T.G., Stouthamer, E., Cohen, K.M., 2022. Planform architecture, meander evolution and grain-size variability of a deltaic channel belt in the Rhine-Meuse delta, The Netherlands. *Sedimentology*, 69(7), 2844—2866.

Wu, W.T., Zhao, J.Z., Wei, X.S., Wang, Y., Zhang, J., Wu, H.Y., Li, J., 2022. Evaluation of gas-rich "sweet-spot" and controlling factors of gas—water distribution in tight sandstone gas provinces: An example from the Permian He8 Member in Sulige Gas Province, central Ordos Basin, Northern China. *Journal of Asian Earth Sciences*, 227, 105098.

Xu, Z.H., Wu, S.H., Plink-Björklund, P., Zhang, T., Yue, D.L., Qian, Q.H., Li, Q., Feng, W.J., 2025. Autocyclic switching processes and architecture of lobes in river-dominated lacustrine deltas. *Journal of Palaeogeography*, 14(1), 126—140.

Yang, H., Fu, J.H., Wei, X.S., Liu, X.S., 2008. Sulige field in the Ordos Basin: Geological setting, field discovery and tight gas reservoirs. *Marine and Petroleum Geology*, 25(4—5), 387—400 (in Chinese with English abstract).

Yang, Z., Wu, S.H., Duan, D.P., Xu, Z.H., Xiong, Q.C., Zhang, Y.F., 2024. Architecture characteristics of distributary channels in shallow water delta plain of the Huagang Formation in Xihu sag, East China Sea. *Journal of Palaeogeography*, 26(3), 525—544 (in Chinese with English abstract).

Yang, R.C., Li, Y., Fan, A.P., Van Loon, A.J., Li, J., Han, Z.Z., Chen, J., 2023. Palaeogeographical development of two merging delta systems (Eocene Shahejie Formation) in the Bohai Bay Basin, E China and implications for hydrocarbon exploration. *Journal of Palaeogeography*, 12(4), 564—586.

Yin, S., Zhao, J.Z., Wu, Z.H., Ding, W.L., 2018. Strain energy density distribution of a tight gas sandstone reservoir in a low-amplitude tectonic zone and its effect on gas well productivity: A 3D FEM study. *Journal of Petroleum Science and Engineering*, 170, 89—104.

Yue, D.L., Hu, G.Y., Li, W., Fan, T.E., Hu, J.J., Qiao, H.L., 2018. Meandering fluvial reservoir architecture characterization method and application by combining well logging and seismic data: A case study of QHD32-6 oilfield. *China Offshore Oil and Gas*, 30(1), 99—109.

Yue, D.L., Li, W., Wang, W.R., Sun, P.K., Wu, S.H., Xu, Z.H., Liu, L., Wu, D.G., Qu, L.B., Ren, K.Y., Lin, J., Zhang, S.Q., 2025a. Advances and perspectives in intelligent characterization and modeling of clastic reservoirs. *Journal of Palaeogeography*, 27(4), 903—923.

Yue, D.L., Li, W., Wang, W.R., Wu, S.H., Li, H.H., Liu, J.Y., Liu, L., Xu, Z.M., Lin, J., Wu, G.Z., 2025b. Advances and prospects of meandering river sedimentary architecture research. *Earth Science Frontiers*, 32(5), 113—130.

Zeng, C., Yin, T.J., Song, Y.K., 2017. Experimental on numerical simulation of the impact of lake level plane fluctuation on shallow water delta. *Earth Science*, 42(11), 2095—2104.

Zhang, X.H., Leonardi, N., Donatelli, C., Fagherazzi, S., 2020. Divergence of sediment fluxes triggered by sea-level rise will reshape coastal bays. *Geophysical Research Letters*, 47(13).

Zhao, C.F., Yu, X.H., Fu, C., Han, X.Q., Du, Y.H., 2019. Control factors and evolution progress of depositional system transition from meandering river delta to braided river delta: Case study of Shan2 member to He8 member, Ordos Basin. *Acta Sedimentologica Sinica*, 37(4), 768—784 (in Chinese with English abstract).

Zhu, P., Ma, T., Wang, X., Li, X.W., Dong, Y.X., Yang, W.M., Teng, Z.D., 2023. Wavelet transform coupled with Fischer plots for sequence stratigraphy: A case study in the Linxing area, Ordos Basin, China. *Geoenergy Science and Engineering*, 231, 212306.

Zhu, W.L., Wu, S.H., Yin, Z.J., Han, T., Wu, Y.M., Liu, Y., Feng, W.J., Luo, Y.N., Cao, C., 2016. Braided river delta outcrop architecture: A case study of Triassic Huangshanjie Formation in Kuche depression, Tarim Basin, NW China. *Petroleum Exploration and Development*, 43(3), 528—536.

Zhu, X.M., Li, S.L., Wu, D., Zhu, S.F., Dong, Y.L., Zhao, D.N., Wang, X.L., Zhang, Q., 2017. Sedimentary characteristics of shallow-water braided delta of the Jurassic, Junggar basin, Western China. *Journal of Petroleum Science and Engineering*, 149, 591—602.

Zheng, R.C., Yin, S.M., Peng, J., 2000. Sedimentary dynamic analysis of sequence structure and stacking pattern of base-level cycle. *Acta Sedimentologica Sinica*, 18(3), 369—375 (in Chinese with English abstract).

Appendix A. Supplementary data

Supplementary data to this article can be found online at https://doi.org/10.1016/j.jop.2026.100368.